Phase matching with Tamm plasmons for enhanced second- and third-harmonic generation

B. I. Afinogenov,[1,*] A. A. Popkova,[1] V. O. Bessonov,[1,†] B. Lukyanchuk,[1,2] and A. A. Fedyanin[1,‡]

[1]*Faculty of Physics, Lomonosov Moscow State University, Moscow 119991, Russia*
[2]*Data Storage Institute, A*STAR (Agency for Science, Technology and Research), 138634 Singapore*

We demonstrate that the intensity of optical second and third harmonics generated in a one-dimensional photonic crystal–thin metal film sample is greatly enhanced in the presence of Tamm plasmons. The emergence of a localized optical Tamm state means that the local density of photonic states is resonantly enhanced at the interface of photonic crystal and metal within the vicinity of the excitation wavelength. When the fundamental radiation spectrum overlaps with the Tamm mode, the efficiency of the second-harmonic generation was enhanced by two orders of magnitude as compared with a bare metal film. In the case of the off-resonant fundamental radiation and the second-harmonic wavelength overlapping with the Tamm plasmon mode, the conversion efficiency increased by one order of magnitude. The overall intensity of the third-harmonic generation was enhanced by almost five orders of magnitude in the phase-matching conditions. In this case the fundamental radiation resonates with the fundamental Tamm plasmon, while the third-harmonic radiation resonates with the third-order Tamm plasmon.

I. INTRODUCTION

Control over spontaneous emission is a cardinal challenge for manufacturing LEDs, lasers, and other imaging devices. Numerous methods to tailor the emission rate of a light source using its environment have been widely investigated since the pioneering article was published by Purcell [1]. Placing the system into a cavity allows for damping or amplifying the emission in the desired direction or at the required wavelength [2,3]. Several groups reported on fabricating the low-threshold lasers with various key substances: quantum dots [4,5], quantum boxes [6], and the carbon nanotubes [7] placed in plasmonic or photonic crystals. The formalism of the Purcell effect can also be expanded up to nonlinear emission, e.g., to the optical-harmonics generation, when the radiation intensity enhances in the Purcell regime due to the increase of the local density of photonic states (LDOS) at the cavity frequencies. LDOS is directly related to the local field factor (LFF) denoting the magnitude ratio between the free-space field and the local field in the structure [8]. As for the process of optical-harmonics generation in dipole approximation, the electric far field of the emitted nth optical-harmonic radiation $E(n\omega)$ depends on the free-space pump field $E(\omega)$ as

$$E(n\omega) = L(n\omega)L^n(\omega) \cdot \hat{\chi}^{(n)} E^n(\omega), \qquad (1)$$

where $\hat{\chi}^{(n)}$ is the nth order nonlinear susceptibility, $L(\omega)$ and $L(n\omega)$ are LFFs for the fundamental and nth harmonic radiation, respectively. According to the equation, $E(n\omega)$ is strongly amplified if either $L(\omega)$ or $L(n\omega)$ is enhanced. Intensities of both the second and third harmonics (SH and TH) are shown to be enhanced as the fundamental LFF is increased in the presence of the localized electromagnetic field modes, such as surface and localized plasmons [9,10] or microcavity modes in photonic crystals (PCs) [11–14]. Enhancement of the multiple order LFF in photonic or plasmonic crystals leads to the enhancement of second-harmonic generation [15,16] and Kerr effect [17]. When both LFFs are enhanced, the phase-matching conditions appear to be satisfied. It was shown that phase-matched optical harmonics generation in photonic crystals could be achieved through the interplay of two mechanisms: localizing fundamental field at the microcavity mode inside the fundamental photonic bandgap (PBG) and increasing the photonic LDOS at harmonic frequency in higher-order resonances [18,19]. Similar techniques have been recently proposed to enhance second-harmonic generation in plasmonic metamaterials [20].

Tamm plasmons (TPs) are surface electromagnetic states emerging at the interface between a one-dimensional photonic crystal (distributed Bragg reflector) and metal [21]. In contrast to the surface plasmon polaritons, TPs can be excited at any angle of incidence via direct optical illumination for both TE and TM polarizations of the incoming light [22–24]. Engineering the geometry of PC/metal sample allows for tuning the TP resonance wavelength in a broad spectral range. The spatial localization of the electromagnetic field at the interface between PCs and metal film can lead to the nonlinear-optical effects greatly enhanced [25], e.g., SH intensity generated in the PC/metal sample [26]. Hybrid states of TPs and microcavity [27] and exciton [28–30] and surface plasmon [31] modes were also thoroughly studied. Energy transfer between the TP mode and the excitations under consideration was used to create low-threshold lasers, tunable sensors, and integrated circuits [32–34].

In this paper, we report the observation of optical second- and third-harmonic generation enhancement in metal/photonic crystal structures in the presence of Tamm plasmons. Enhancement of the second-harmonic generation (SHG) is ensured either by the fundamental field localized in the TP mode

───────
*afinogenov@nanolab.phys.msu.ru
†Also at: Frumkin Institute of Physical Chemistry and Electrochemistry, Russian Academy of Sciences, Moscow 119071, Russia.
‡fedyanin@nanolab.phys.msu.ru

(resonant fundamental radiation) or by a rise in the photonic LDOS at the SH frequency triggered by the TP mode excitation (resonant second-harmonic radiation). As far as the third-harmonic generation (THG) is concerned, the phase-matching conditions can be achieved only when the aforementioned conditions are realized simultaneously.

II. EXPERIMENT

Two types of samples were prepared by means of the magnetron sputtering technique. The former (type 1) was a $(SiO_2/Ta_2O_5)_7$ distributed Bragg reflector formed by quarter-wavelength-thick layers with thicknesses of 130 and 92 nm, respectively. Samples in the second set (type 2) had a structure $(ABA*B*)_5$, where A and $A*$ stand for SiO_2 layers with thicknesses of 240 and 284 nm, and B and $B*$ stand for Ta_2O_5 layers with thicknesses of 164 and 194 nm, respectively. Refractive indices and layer thicknesses were defined using scanning electron microscopy and ellipsometry techniques. All the samples were covered by a thermally evaporated 30-nm-thick silver film. To prevent ageing of the silver film, a protective 10-nm-thick Al_2O_3 layer was deposited on top of the metal. Samples were numerically designed through transfer-matrix technique [35] to yield the following TP resonance wavelengths: 800 nm at $20°$ angle of incidence for type-1 samples and 1560 and 520 nm for the fundamental and third-order TP resonances in type-2 samples.

A femtosecond Er:fiber laser served as a source of radiation further passing through two Glan-Taylor prisms, which were used to control power and polarization of the fundamental radiation. The beam was focused to a 40-μm spot at the sample. The corresponding peak intensity of the fundamental radiation was 1 GW/cm^{-2}. The sample was mounted on a rotational stage allowing control of the angle of incidence with a $0.01°$ accuracy. The optical harmonics radiation, generated in the sample in a transmission geometry, was collimated, filtered from the fundamental radiation, and further passed through an analyzer and detected with a photomultiplier tube. A sketch of the experiment is shown in Fig. 1(a). The setup allowed for studying SHG and THG in any combination of fundamental and optical-harmonic radiation polarizations. However, the largest intensities of second- and third-optical harmonics were obtained when both the fundamental and optical-harmonic beams were TM polarized.

For the numerical simulations we used a nonlinear transfer matrix method [35] to calculate the angular dependence of SH and TH intensities, generated in the sample and in the bare silver film. An inversion symmetry is typical of all the sample layers due to the method they were manufactured by. It means that bulk dipole second-harmonic generation is forbidden. Therefore, the only source of second-order optical nonlinearity are thin regions near the interfaces of layers. To estimate the effective surface second-order susceptibilities of sample layers, SH intensities were measured from bare PC and bare silver film. The obtained results have shown that intensity of SH generated in the PC is at least two orders of magnitude less than the one from the silver film. Thus, while analyzing experimental data, second-order nonlinearity of the PC was neglected. For the calculations of the SHG efficiency we assumed that the only sources of SH are 1-nm-thick boundary
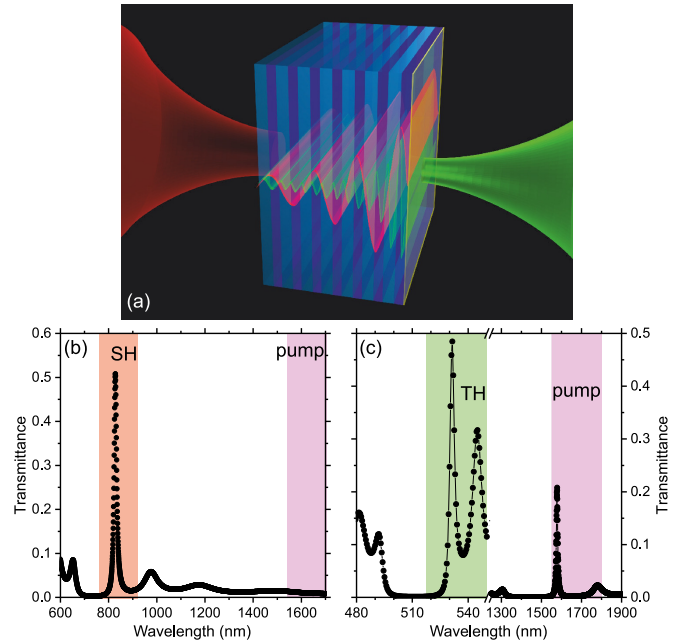

FIG. 1. (a) Sketch of the experiment. Transmittance spectrum of type 1 (b) and type 2 (c) samples measured at normal incidence. Shaded areas indicate the regions which are spectrally scanned with the change of the angle of incidence from $0°$ to $60°$.

layers of metal. On the contrary, bulk $\hat{\chi}^{(3)}$ is nonzero for all the layers composing the structure. According to Refs. [36,37], third-order susceptibility is 2×10^{-11} esu for silver, 2×10^{-14} esu for SiO_2, and 3×10^{-13} esu for Ta_2O_5. At the same time, the silver thickness is 150 times smaller than the one of PC. Thus, both PC and silver almost equally contribute to the third-harmonic generation in the sample and bulk third-order susceptibilities of all the layers were considered in the calculations.

III. RESULTS AND DISCUSSION

Figure 1(b) shows the transmittance spectrum of type-1 sample at a normal incidence. It exhibits a photonic band gap (PBG) between 650 and 950 nm with a sharp peak at 820 nm inside the PBG associated with the TP resonance. When the angle of incidence is increased, the whole spectrum blueshifts. Figure 1(c) shows the transmittance spectrum of the type-2 sample at a normal incidence. The first-order PBG of the sample lies between 1250 and 1750 nm and the first-order TP resonance emerges at 1580 nm at normal incidence. The third-order PBG lies between 490 and 550 nm with the third-order TP resonance at 532 nm. In addition to the transmittance spectroscopy, the TP nature of the mentioned resonances was verified by numerical calculations of the electromagnetic field distributions at the resonant wavelengths.

A. Case of a single-resonant second-harmonic radiation

In case of single resonance, only one of the local-field factors in Eq. (1) was amplified: either $L(\omega)$ for the resonant pump or $L(2\omega)$ for the resonant SH. The electromagnetic field in the TP mode is spatially localized near the interface between PC and metal. It peaks at the center of the PC topmost layer and decays as the distance from the interface increases.
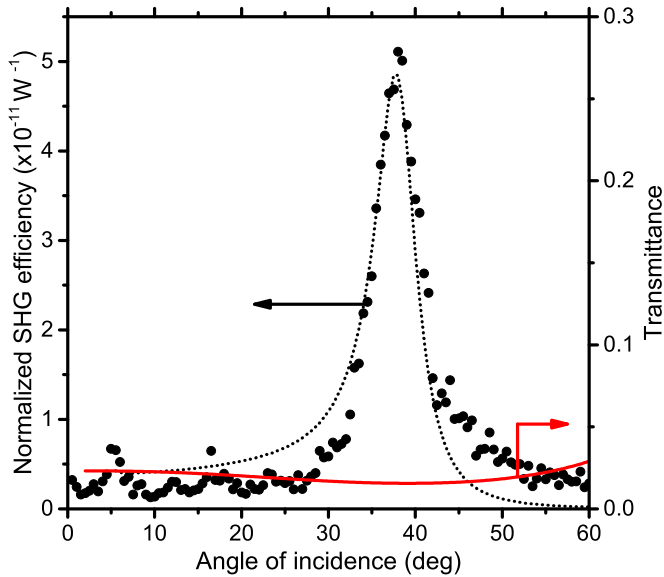
FIG. 2. Angular dependence of normalized efficiency of the second-harmonic generation in type-1 sample (dots), numerical calculations of the SHG efficiency (dotted curve), and transmittance of the fundamental radiation with the wavelength of 1560 nm (red curve).

FIG. 3. Normalized THG efficiency in type-2 sample, measured in a pp geometry (dots). The transmittance of a fundamental radiation at the wavelength of 1560 nm (red curve). Inset shows the TH intensity vs fundamental power in log-log scale.

According to numerical calculations, fundamental LFFs at the inner metal surface at the wavelength of the TP resonance are $L^{Me}(\omega) = 0.21$ and $L^{PC}(\omega) = 0.89$ in a bare silver film and PC/metal sample, respectively. However, LFF for the second-harmonic radiation is slightly damped in the PC/metal sample $L^{PC}(2\omega) = 0.26$ as compared with an LFF in a bare silver film $L^{Me}(2\omega) = 0.35$. Overall, a 180-times increase of the SH intensity generated in the PC/metal sample is obtained when the fundamental electric field in the nonlinear layer of the sample is fourfold enhanced. The maximum normalized SHG efficiency (SH power divided by the square of the pump power) obtained in the experiment was 2.4×10^{-9} W^{-1}. Explicit results of the resonant fundamental radiation case study are presented in our previous paper [26].

The case of the resonant second-harmonic LFF is less intuitive, since fundamental radiation is not localized in the nonlinear layer under such conditions. However, the excitation of the Tamm plasmon leads to the enhanced $L(2\omega)$ when frequency of the second-harmonic radiation matches the TP frequency. In the present experiment, the type-1 sample was pumped by a p-polarized radiation with a central wavelength at 1560 nm. Figure 2 shows transmittance of the type-1 sample at the fundamental wavelength versus the angle of incidence.

The pump wavelength lies within the PBG, yet silver has a high absorbance at the corresponding wavelengths, and the resultant transmittance is relatively low. No resonant peculiarities were observed in the transmittance spectrum; the $L(\omega)$ at the silver surface is 0.1. The $L(\omega)$ in a bare silver film appears to be of the same order, namely equal to 0.09; it means that no enhancement of the pump field is observed in this case. Measurements of SHG were performed in a pp combination of fundamental and SH beam polarizations. Figure 2 shows the normalized SHG efficiency with dots. Out of the resonance, SH intensity is almost negligible, whereas in the vicinity of the TP mode SH intensity increases drastically. At 38° angle of inci-
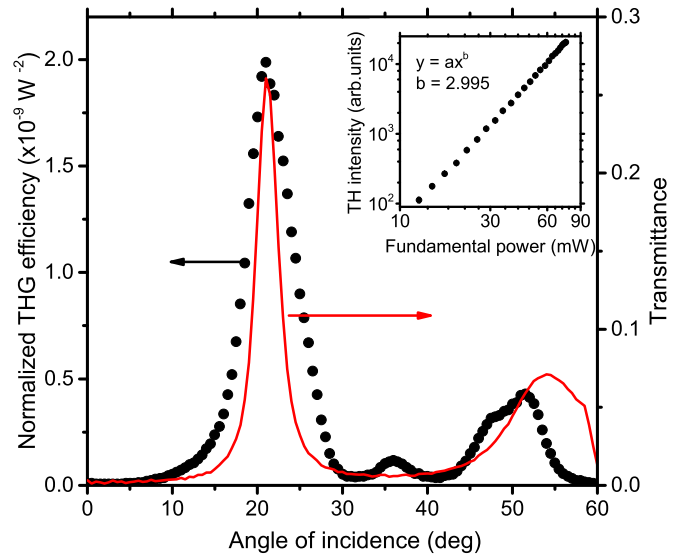
dence, SHG efficiency reaches the value of 5.3×10^{-11} W^{-1}, which corresponds to the 23-fold enhancement as compared to a bare silver film.

In the absence of the fundamental field localization, resonant SHG enhancement is related to the increase in LFF at the SH wavelength. The nonlinear transfer matrix method was used to calculate the angular dependence of SH intensities, generated in the sample and in the silver film. The obtained results are presented in Fig. 2 with the dotted curve. In the case with resonant second harmonic the maximum observed SHG enhancement factor is only 23, which is smaller than with the resonant pump by one order of magnitude. However, since the fundamental field is not localized at a metal film, higher intensities can be pumped in the sample without its destruction. This phenomenon may be particularly useful in sensing applications when the active layer is embodied underneath the metal film.

B. Case of a double-resonant third harmonic generation

The phase matching for the third-harmonic radiation is realized by enhancing $L(\omega)$ and $L(3\omega)$ simultaneously due to the excitation of the fundamental and third-order Tamm plasmons. A specially designed type-2 structure exhibits Tamm plasmon resonances at 1560 nm, and at a tripled frequency 520 nm at a 20° angle of incidence. The transmittance of the studied structure versus the angle of incidence at 1560 nm is shown in Fig. 3 with the solid curve.

Under normal incidence the wavelength of 1560 nm corresponds to the center of a fundamental PBG [see Fig. 1(c)]; at that, the transmittance is as low as 0.01. As the angle of incidence increases, PBG and TP modes shift towards higher frequencies; the growth in transmittance can be observed as the fundamental wavelength approaches the TP resonance. As the angle of incidence is increased further and goes beyond 45°, the long-wave edge of PBG appears and transmittance in-
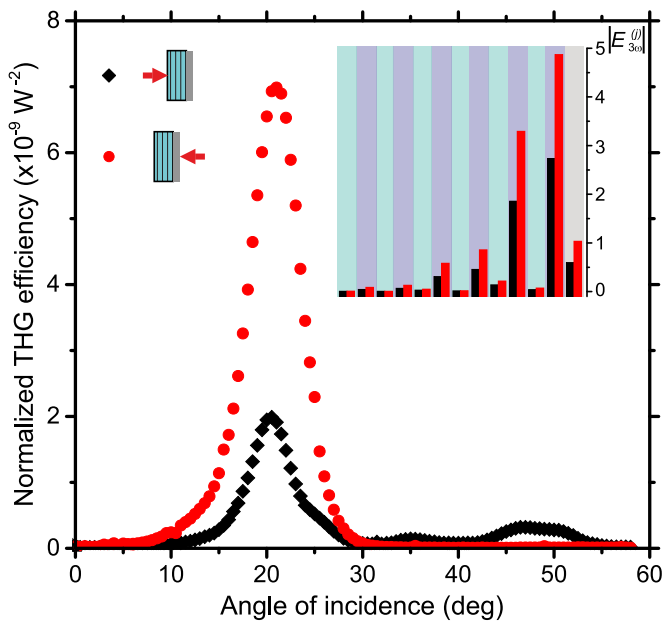
FIG. 4. Angular dependence of the normalized THG efficiency in a PC/metal sample in *pp*-polarization combination. Black diamonds correspond to the case when the PC side of the sample faces the fundamental radiation; red dots correspond to the case when the metal layer faces the fundamental radiation. Inset shows magnitudes of partial contributions of individual layers to the third-harmonic field calculated at 21° angle of incidence for the described orientations of the sample.
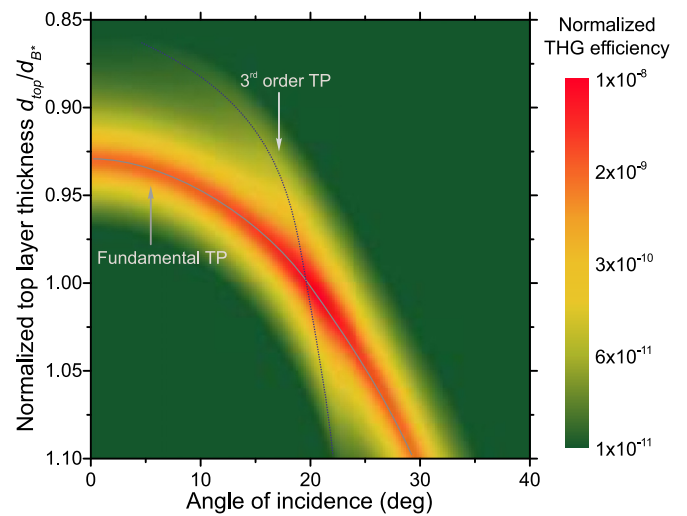

FIG. 5. Calculated dependence of THG efficiency vs angle of incidence and thickness of the topmost layer of photonic crystal normalized to the thickness of the regular $B*$ layer.

creases again. Dots in Fig. 3 represent the normalized THG efficiency in the type-2 sample in the *pp* combination of fundamental and TH polarizations measured in the transmission geometry. The sample faced the incident radiation with a PC. Three peaks are observed in the angular dependence of the TH intensity at 21°, 36°, and 52°. The increase of THG efficiency at 52° results from the enhancement in $L(3\omega)$ near the edge of PBG. The peak at 36° appears due to the increase of $L(3\omega)$ when the harmonic radiation spectrally passes the waveguide mode observed in Fig. 1(c) at 545 nm. Sharp resonance at 21° is associated both to the fundamental electromagnetic field localization in the TP mode near the metal boundary and to the resonant increase of $L(3\omega)$ induced by the third-order TP mode excitation. As compared to a bare silver film, on reaching its peak TH intensity from PC/metal structure is increased by a factor of 1.5×10^4.

The shape of the THG efficiency angular spectrum depends largely on how the sample is oriented in reference to the incident beam. Figure 4 shows THG efficiency in the structure with a metal layer facing the incident fundamental radiation along with the data from Fig. 3. In the silver-faced case, intensity of the TP-associated peak is threefold increased, while other peaks are significantly damped. To understand the observed behavior we calculated partial contributions from individual layers of the sample to the third-harmonic field. The results are shown in the inset of Fig. 4. It can be noted that in the metal-faced orientation every layer of the sample generates almost twice as much third-harmonic field as in the PC-faced orientation. This arises from the difference in conditions of a

multipath interference of the fundamental radiation, and thus the different fundamental field distributions.

Fundamental and third-order Tamm plasmon resonances overlap only if PC parameters, such as thicknesses d_i or refractive indices n_i of constituting layers, are at their optimal values or very close to them. To check up that double-resonance conditions are realized in the sample, we defined n_i and d_i for the sample using scanning electron microscopy and ellipsometry techniques. Then, the obtained values were used to calculate TH intensity. Since the angular position of the TP resonance is particularly sensitive to the thickness of the topmost layer of a photonic crystal d_{top} [23], this value was chosen to be a variable parameter. The calculations were made to study the influence of the fundamental and third-order peaks overlapping on the efficiency of the third harmonic generation. In addition, a variation in the thickness of the topmost layer does not significantly change the amount of nonlinear material, which is essential to compare THG efficiencies under different conditions. Figure 5 shows the normalized THG efficiency versus the angle of incidence and the topmost layer thickness. The latter is represented as a fraction of the regular $B*$ layer thickness. Fundamental radiation is assumed to be incident from the metal side of the sample. A sharp high-amplitude peak marked with a solid curve in Fig. 5 is associated with the fundamental TP resonance and the THG enhancement triggered by the localizing the fundamental field in nonlinear layers. The d_{top} significantly influences angular position of the peak. At the thickness of 1.1 (corresponding to 210-nm thick top layer) the peak is observed at 29°, and it is accompanied by a weaker peak at 22°, which is caused by the increase in $L(3\omega)$ at the third-order TP resonance. With the decrease of d_{top} the two peaks approach each other. When d_{top} does not differ from d_{B*} and equals 194 nm, the peaks are excited at the same angle of incidence 21°, which corresponds to the experimental conditions. Overall, in the case of resonances overlapping, TH intensity is increased by an additional order of magnitude as compared to the single-resonant case.

IV. CONCLUSIONS

In conclusion, we have realized three configurations of optical-harmonics generation in PC/metal structures supporting Tamm plasmon excitation. It has been shown that second- and third-harmonic generation may be enhanced either by directly localizing the fundamental field at the metal surface or by enhancing the local density of photonic states in the TPP mode at the frequency of optical harmonic. Normalized conversion efficiencies to the second-harmonic are 2.4×10^{-9} W^{-1} and 5.3×10^{-11} W^{-1} in the cases of fundamental and second-harmonic resonances, respectively, with the corresponding enhancement factors equating 180 and 23. As for the third-harmonic generation, a phase matching can be achieved with the 6×10^4 enhancement factor of TH intensity, which corresponds to the conversion efficiency of 7×10^{-9} W^{-2}. Since conditions of the TP excitation and the TP phase matching are highly susceptible to the refractive index of the environment, we believe the results are particularly useful to develop background-free detectors and sensors based on Tamm plasmons.

[1] E. M. Purcell, Phys. Rev. **69**, 681 (1946).

[2] S. Noda, M. Fujita, and T. Asano, Nat. Photon. **1**, 449 (2007).

[3] H. Cang, Y. Liu, Y. Wang, X. Yin, and X. Zhang, Nano Lett. **13**, 5949 (2013).

[4] H. Altug, D. Englund, and J. Vučković, Nat. Phys. **2**, 484 (2006).

[5] S. Wu, S. Buckley, J. R. Schaibley, L. Feng, J. Yan, D. G. Mandrus, F. Hatami, W. Yao, J. Vučković, and A. Majumdar, Nature (London) **520**, 69 (2015).

[6] J. M. Gérard, B. Sermage, B. Gayral, B. Legrand, E. Costard, and V. Thierry-Mieg, Phys. Rev. Lett. **81**, 1110 (1998).

[7] Y. Zakharko, A. Graf, S. P. Schiessl, B. Hähnlein, J. Pezoldt, M. C. Gather, and J. Zaumseil, Nano Lett. **16**, 3278 (2016).

[8] L. Novotny and B. Hecht, *Principles of Nano-Optics* (Cambridge University Press, Cambridge, England, 2012).

[9] S. Kim, J. Jin, Y.-J. Kim, I.-Y. Park, Y. Kim, and S.-W. Kim, Nature (London) **453**, 757 (2008).

[10] Y. Zhang, F. Wen, Y.-R. Zhen, P. Nordlander, and N. J. Halas, Proc. Natl. Acad. Sci. USA **110**, 9215 (2013).

[11] T. V. Dolgova, A. I. Maidykovski, M. G. Martemyanov, A. A. Fedyanin, O. A. Aktsipetrov, G. Marowsky, V. A. Yakovlev, and G. Mattei, Appl. Phys. Lett. **81**, 2725 (2002).

[12] M. G. Martemyanov, E. M. Kim, T. V. Dolgova, A. A. Fedyanin, O. A. Aktsipetrov, and G. Marowsky, Phys. Rev. B **70**, 073311 (2004).

[13] I. V. Soboleva, E. M. Murchikova, A. A. Fedyanin, and O. A. Aktsipetrov, Appl. Phys. Lett. **87**, 241110 (2005).

[14] S. Buckley, M. Radulaski, J. Petykiewicz, K. G. Lagoudakis, J.-H. Kang, M. Brongersma, K. Biermann, and J. Vučković, ACS Photon. **1**, 516 (2014).

[15] J. Martorell, R. Vilaseca, and R. Corbalan, Appl. Phys. Lett. **70**, 702 (1997).

[16] J. Martorell, R. Vilaseca, A. Corbalan, R. Molinos-Gomez, M. Maymo, X. Vidal, D. Velasco, J. Martorell, and F. Lopez-Calahorra, Adv. Mater. **19**, 3814 (2007).

[17] P. Bermel, A. Rodriguez, J. D. Joannopoulos, and M. Soljačić, Phys. Rev. Lett. **99**, 053601 (2007).

[18] C.-H. Xue, H.-T. Jiang, H. Lu, G.-Q. Du, and H. Chen, Opt. Lett. **38**, 959 (2013).

[19] W. Lu, P. Xie, Z.-Q. Zhang, G. K. L. Wong, and K. S. Wong, Opt. Express **14**, 12353 (2006).

[20] M. Celebrano, X. Wu, M. Baselli, S. Großmann, P. Biagioni, A. Locatelli, C. De Angelis, G. Cerullo, R. Osellame, B. Hecht, L. Duò, F. Ciccacci, and M. Finazzi, Nat. Nanotechnol. **10**, 412 (2015).

[21] J. A. Gaspar-Armenta and F. Villa, J. Opt. Soc. Am. B **20**, 2349 (2003).

[22] M. E. Sasin, R. P. Seisyan, M. A. Kalitteevski, S. Brand, R. A. Abram, J. M. Chamberlain, A. Y. Egorov, A. P. Vasil'ev, V. S. Mikhrin, and A. V. Kavokin, Appl. Phys. Lett. **92**, 251112 (2008).

[23] M. Kaliteevski, I. Iorsh, S. Brand, R. A. Abram, J. M. Chamberlain, A. V. Kavokin, and I. A. Shelykh, Phys. Rev. B **76**, 165415 (2007).

[24] B. I. Afinogenov, A. A. Popkova, V. O. Bessonov, and A. A. Fedyanin, Appl. Phys. Lett. **109**, 171107 (2016).

[25] I. V. Iorsh, P. A. Belov, A. A. Zharov, and I. V. Shadrivov, and Y. S. Kivshar, Phys. Rev. A **86**, 023819 (2012).

[26] B. I. Afinogenov, V. O. Bessonov, and A. A. Fedyanin, Opt. Lett. **39**, 6895 (2014).

[27] R. Brückner, M. Sudzius, S. I. Hintschich, H. Fröb, V. G. Lyssenko, and K. Leo, Phys. Rev. B **83**, 033405 (2011).

[28] C. Symonds, G. Lheureux, J.-P. Hugonin, J.-J. Greffet, J. Laverdant, G. Brucoli, A. Lemaître, P. Senellart, and J. Bellessa, Nano Lett. **13**, 3179 (2013).

[29] T. Braun, V. Baumann, O. Iff, S. Höfling, C. Schneider, and M. Kamp, Appl. Phys. Lett. **106**, 041113 (2015).

[30] M. Salewski, S. V. Poltavtsev, Yu. V. Kapitonov, J. Vondran, D. R. Yakovlev, C. Schneider, M. Kamp, S. Höfling, R. Oulton, I. A. Akimov, A. V. Kavokin, and M. Bayer, Phys. Rev. B **95**, 035312 (2017).

[31] B. I. Afinogenov, V. O. Bessonov, A. A. Nikulin, and A. A. Fedyanin, Appl. Phys. Lett. **103**, 061112 (2013).

[32] R. Brückner, A. Zakhidov, R. Scholz, M. Sudzius, S. Hintschich, H. Fröb, V. Lyssenko, and K. Leo, Nat. Photon. **6**, 322 (2012).

[33] G. Lheureux, S. Azzini, C. Symonds, P. Senellart, A. Lemaître, C. Sauvan, J.-P. Hugonin, J.-J. Greffet, and J. Bellessa, ACS Photon. **2**, 842 (2015).

[34] B. Auguié, M. C. Fuertes, P. C. Angelomé, N. L. Abdala, G. J. Soler Illia, and A. Fainstein, ACS Photon. **1**, 775 (2014).

[35] D. Bethune, J. Opt. Soc. Am. B **6**, 910 (1989).

[36] R. W. Boyd, *Nonlinear Optics*, (Academic, New York, 2008).

[37] R. Y. Chen, M. D. Charlton, and P. G. Lagoudakis, Opt. Lett. **34**, 1135 (2009).